frontiers in Marine Science

ORIGINAL RESEARCH
published: 01 March 2018
doi: 10.3389/fmars.2018.00061

Distinct Siderophores Contribute to Iron Cycling in the Mesopelagic at Station ALOHA

*Randelle M. Bundy[1,2], Rene M. Boiteau[1,3], Craig McLean[1], Kendra A. Turk-Kubo[4], Matt R. McIlvin[1], Mak A. Saito[1], Benjamin A. S. Van Mooy[1] and Daniel J. Repeta[1]**

[1] Marine Chemistry and Geochemistry, Woods Hole Oceanographic Institution, Woods Hole, MA, United States, [2] School of Oceanography, University of Washington, Seattle, WA, United States, [3] Environmental Molecular Sciences Laboratory, Pacific Northwest National Laboratory, Richland, WA, United States, [4] Physical and Biological Sciences, University of California, Santa Cruz, Santa Cruz, CA, United States

OPEN ACCESS

Edited by:
Samuel Wilson,
University of Hawaii at Manoa,
United States

Reviewed by:
Martha Gledhill,
University of Southampton,
United Kingdom
Oliver Baars,
Princeton University, United States

***Correspondence:**
Daniel J. Repeta
drepeta@whoi.edu

Specialty section:
This article was submitted to Aquatic Microbiology, a section of the journal Frontiers in Marine Science

Received: 07 December 2017
Accepted: 09 February 2018
Published: 01 March 2018

Citation:
Bundy RM, Boiteau RM, McLean C, Turk-Kubo KA, McIlvin MR, Saito MA, Van Mooy BAS and Repeta DJ (2018) Distinct Siderophores Contribute to Iron Cycling in the Mesopelagic at Station ALOHA. Front. Mar. Sci. 5:61. doi: 10.3389/fmars.2018.00061

The distribution of dissolved iron (Fe), total organic Fe-binding ligands, and siderophores were measured between the surface and 400 m at Station ALOHA, a long term ecological study site in the North Pacific Subtropical Gyre. Dissolved Fe concentrations were low throughout the water column and strong organic Fe-binding ligands exceeded dissolved Fe at all depths; varying from 0.9 nmol L^{-1} in the surface to 1.6 nmol L^{-1} below 150 m. Although Fe does not appear to limit microbial production, we nevertheless found siderophores at nearly all depths, indicating some populations of microbes were responding to Fe stress. Ferrioxamine siderophores were most abundant in the upper water column, with concentrations between 0.1 and 2 pmol L^{-1}, while a suite of amphibactins were found below 200 m with concentrations between 0.8 and 11 pmol L^{-1}. The distinct vertical distribution of ferrioxamines and amphibactins may indicate disparate strategies for acquiring Fe from dust in the upper water column and recycled organic matter in the lower water column. Amphibactins were found to have conditional stability constants (log $K^{cond}_{FeL_1,Fe'}$) ranging from 12.0 to 12.5, while ferrioxamines had much stronger conditional stability constants ranging from 14.0 to 14.4, within the range of observed L_1 ligands by voltammetry. We used our data to calculate equilibrium Fe speciation at Station ALOHA to compare the relative concentration of inorganic and siderophore complexed Fe. The results indicate that the concentration of Fe bound to siderophores was up to two orders of magnitude higher than inorganic Fe, suggesting that even if less bioavailable, siderophores were nevertheless a viable pathway for Fe acquisition by microbes at our study site. Finally, we observed rapid production of ferrioxamine E by particle-associated bacteria during incubation of freshly collected sinking organic matter. Fe-limitation may therefore be a factor in regulating carbon metabolism and nutrient regeneration in the mesopelagic.

Keywords: iron, siderophores, Station ALOHA, organic ligands, iron limitation

INTRODUCTION

Iron (Fe) is an essential trace metal for many cellular processes in marine phytoplankton and bacteria, including nitrogen fixation and photosynthesis (Morel and Price, 2003). The Hawaii Ocean Time-series (HOT) at Station ALOHA has been a major study site to evaluate the annual and interannual variability in Fe chemistry and its influence on oligotrophic marine ecosystems. These time-series measurements have revealed a dynamic Fe cycle, with atmospheric dust deposition and mixing of deeper waters into the photic zone acting as a fluctuating source of bioavailable Fe (Boyle et al., 2005; Fitzsimmons et al., 2015). Although Fe is not considered to be a limiting nutrient in the oligotrophic North Pacific, competition for Fe among microorganisms may still impact community dynamics (Rue and Bruland, 1995; Johnson et al., 2007; Fitzsimmons et al., 2015). *Prochlorococcus* for example, the dominant photoautotroph at Station ALOHA, can thrive even under the low Fe conditions in the oligotrophic ocean (Johnson and Lin, 2009; Thompson et al., 2011). However, larger, more transiently abundant taxa such as diatoms and nitrogen fixing photoautotrophs such as *Trichodesmium* spp. often have high cellular Fe quotas (Berman-Frank et al., 2001; Kustka et al., 2003; Roe et al., 2012). These microbes could face Fe stress at times when the atmospheric delivery of Fe is low. Indeed, Fitzsimmons et al. (2015) observed an increase in internalization of Fe by diatoms following Fe inputs to the region either from dust or mesoscale eddies (Rue and Bruland, 1995; Johnson et al., 2007; Fitzsimmons et al., 2015). While oligotrophic ecosystems such as the one at Station ALOHA may not show a chlorophyll *a* or biomass response to Fe amendments, the traditional way by which Fe limitation is defined, the cycling of Fe within the community may nevertheless be important in determining the success of specific groups of microbes and for the ecosystem as a whole.

Confounding our understanding of Fe cycling is the observation that almost all dissolved Fe in the ocean is associated with organic ligands of largely unknown identity (see review by Gledhill and Buck, 2012). Voltammetric techniques, such as competitive ligand exchange adsorptive cathodic stripping voltammetry (CLE-ACSV), have been used to measure the concentrations and binding strengths of Fe-binding organic ligands across ocean basins (GEOTRACES; Buck et al., 2015, in press; Gerringa et al., 2015), on smaller seasonal studies of Fe cycling (Bundy et al., 2014; Fitzsimmons et al., 2015), and on numerous process cruises completed over the past two decades (Gledhill and Buck, 2012). These studies have established that nanomolar concentrations of Fe-binding organic compounds occur throughout the water column, and that a fraction of these ligands have an extremely high affinity for Fe (Gledhill and Buck, 2012; Buck et al., 2015, in press; Gerringa et al., 2015; Bundy et al., 2016). These ligands are generally referred to as either strong (L_1-type) or weaker (L_2-type) ligands, though several additional ligand classes have also been reported (Gledhill and Buck, 2012; Bundy et al., 2014, 2016; Buck et al., 2015). These ligands may be the by-product of routine organic matter cycling by microbes, however based on their similar binding strengths for Fe, it has been inferred that a fraction of natural ligands is composed of siderophores, high-affinity organic Fe-binding ligands used by bacteria to acquire Fe from their environment (Haygood et al., 1993; Reid et al., 1993; Butler, 1998, 2005; Hutchins et al., 1999; Martinez et al., 2000, 2001, 2003; Ito and Butler, 2005; Vraspir and Butler, 2009; Boiteau et al., 2013, 2016; Boiteau and Repeta, 2015). The presence of siderophores within the Fe-ligand pool is significant, in that it entails a direct intervention in dissolved Fe cycling and speciation by marine microbes.

Recent advances in mass spectrometry and sample processing have enabled the picomolar detection of siderophores in seawater (Gledhill et al., 2004; Mawji et al., 2008; Velasquez et al., 2011; Boiteau et al., 2013, 2016; Boiteau and Repeta, 2015), and dissolved siderophores have been successfully characterized from surface waters of the Atlantic (Mawji et al., 2008) and Pacific (Boiteau et al., 2016). CLE-ACSV does not provide molecular-level information on ligand composition and it is not yet known what fraction of the strong ligands in the water column might be siderophores. Very few direct measurements of siderophores have been made in seawater (Mawji et al., 2008; Boiteau et al., 2016). Nevertheless, the distribution and cycling of siderophores can potentially be inferred from the very strong (L_1) class of Fe-binding organic ligands measured by CLE-ACSV. Elevated L_1 concentrations have been found in oceanic regions with elevated macronutrients relative to dissolved Fe (high nitrate:Fe; Buck and Bruland, 2007; Wagener et al., 2008; Ibisanmi et al., 2011; Bundy et al., 2014, 2016) and have also been linked with the subsurface chlorophyll maximum (Rue and Bruland, 1995; van den Berg, 1995; Boye et al., 2001, 2006; Croot et al., 2004; Gerringa et al., 2006, 2008; Tian et al., 2006; Buck and Bruland, 2007; Wagener et al., 2008; Ibisanmi et al., 2011; Bundy et al., 2016), which in many regions of the ocean may be co-limited by Fe and light (Sunda and Huntsman, 1997; Holm-Hansen et al., 2005; Hopkinson et al., 2007; Hopkinson and Barbeau, 2008; Boyd and Ellwood, 2010). L_1 production has also been observed in macronutrient amendment experiments that have evolved into Fe-limiting conditions, or in incubation experiments when external Fe is added (Buck et al., 2007, 2010; Kondo et al., 2008; King and Barbeau, 2011; Bundy et al., 2014, 2016; Adly et al., 2015). CLE-ACSV-based studies therefore suggest a potentially broad role for siderophores in Fe cycling, however, there have been no studies to quantitatively compare mass spectrometric measurements of dissolved siderophores with Fe-binding ligands (L) measured by voltammetric techniques. It is therefore unknown if siderophores are among the strong ligands produced when microbial communities are Fe-limited in experimental mesocosms, or if they are present in regions where Fe is not the primary limiting nutrient.

Here we report the distribution of dissolved siderophores in the water column near Station ALOHA, a well-studied system with respect to microbial community dynamics (Karl and Lukas, 1996; Karl and Church, 2014) and Fe cycling (Boyle et al., 2005; Fitzsimmons et al., 2015). In order to capture a more complete picture of Fe speciation and cycling, we coupled our mass spectrometric analyses of siderophores with measurements of the ligand pool using traditional voltammetry. The profile data is also complemented with an Fe speciation model, as well as an incubation experiment that examines siderophore

production from particle-associated bacteria, in order to inform the mechanisms leading to rapid Fe cycling at Station ALOHA. This work is the first study to date that begins to quantitatively assess the contribution of siderophores to the overall organic pool binding Fe in seawater, and to explore the mechanisms for their depth distributions. The evidence presented also argues that siderophores play a role in the dynamic and rapid cycling of Fe at Station ALOHA by the microbial community, and suggests siderophores may contribute disproportionately to Fe cycling in the mesopelagic in this region.

METHODS

Sampling and Storage

Sampling was done on-board the R/V *Ka'imikai-O-Kanaloa* (KOK) from July 26-August 2, 2015. Water column samples for siderophore analysis were collected from 7 depths in the Station ALOHA circle (22.75 °N, 158 °W; July 28, 2015) using a deckboard Teflon diaphragm pump for the 15 m sample (Cole Parmer) and a trace metal clean X-Niskin rosette (Ocean Test Equipment) for all other depths. Samples for flow cytometry were taken directly from the Niskin bottles, fixed with 0.1% paraformaldehyde, incubated in the dark for 15 min then flash-frozen with liquid nitrogen and stored at −80°C. Samples for macronutrients, dissolved Fe, total Fe-binding ligands, and siderophore analyses were filtered (0.2 μm Acropak 200 capsule filter) into trace metal clean 20 L polycarbonate carboys (Nalgene) and double bagged in heavy duty trash bags before processing. Fe samples were immediately acidified to pH 1.8 with 6 N Optima HCl (4 mL L^{-1}) and stored for 3 months before laboratory analyses. Samples for total Fe-binding ligands (measured by voltammetry) and nutrients were stored frozen at −20°C. Siderophores were extracted on board as described in the section Siderophore Identification in Station ALOHA Seawater, and the solid phase extraction columns were frozen at −20°C.

Nutrients and Flow Cytometry

Dissolved nutrients were analyzed in the Woods Hole Oceanographic Institution Nutrient Analytical Facility using a SEAL AA3 four-channel segmented flow analyzer. Nitrate (nitrate+nitrite), silicate and phosphate were analyzed with 0.01, 0.016, and 0.025 μmol L^{-1} detection limits for each nutrient, respectively. Flow cytometry samples were enumerated for heterotrophic bacteria as well as *Prochlorococcus, Synechococcus,* and photosynthetic picoeukaryote cells using a BD Biosciences Influx Cell Sorter as described in Shilova et al. (2017). *Synechococcus* were enumerated based on the presence of phycoerythrin, and all other non-phycoerythrin cells were identified using forward scatter as a proxy for cell size and red fluorescence (chlorophyll *a* content). Half of the sample was stained with SYBR^{VR} Green I nucleic acid stain (Lonza, Allendale, New Jersey, USA) based on Marie et al. (1999) to determine the abundance of heterotrophic bacteria. Cell count data was processed using FlowJo v10.0.7 (Tree Star, Ashland, Oregon, USA).

Isolation and Purification of Amphibactins From *Vibrio cyclitrophicus 1F-53*

Several *Vibrio* strains containing the non-ribosomal peptide synthases encoding genes putatively identified for amphibactin production (Kem and Butler, 2015; Kem et al., 2015; Boiteau et al., 2016) were cultured in 25 mL Fe-limiting media (2.01 g casamino acids, 0.13 g ultrapure glycerophosphate disodium hydrate, and 1.03 g ultrapure ammonium chloride in 1 L of filtered South Pacific seawater). The strains assessed for amphibactin production included; *Vibrio cyclitrophicus FF75* (FF75), *Vibrio splendidus ZS-139* (ZS-139), *Vibrio tasmaniensis ZS-17* (ZS-17), *Vibrio tasmaniensis 5F-79* (5F-79), and *Vibrio cyclitrophicus 1F-53* (1F-53). Cultures were screened for siderophore production through initial, log, and stationary phases using the chrome azurol S (CAS) colorimetric assay (Schwyn and Neilands, 1987). One liter cultures of *Vibrio cyclitrophicus* 1F-53, the strongest responder to CAS, were harvested during late log phase by centrifuging the cultures and extracting the supernatant onto a polystyrene divinyl benzene (Bond Elut ENV, Agilent Technologies) solid phase extraction (SPE) column. The column was eluted in 10 mL distilled methanol and the eluent reduced in volume to ∼1 mL after drying down for 4 h at 35°C on a SpeedVac concentrator coupled to a refrigerated vapor trap (Thermo Scientific). Siderophores were separated by reverse phase high pressure liquid chromatography (HPLC), using an Agilent 1200 series LC and a C_{18} column (4.2 × 150 mm, 5 μm particle size; Agilent Zorbax), and detected by electrospray ionization quadrupole mass spectrometry (ESI-MS; Agilent 6130 series). Amphibactins were separated using a flow rate of 1 mL min^{-1} using a 98/2 gradient elution (% A/B) for 5 min, 90/10 for 15 min, 2/98 for 10 min, and 98/2 for 1 min (A = LCMS grade H_2O with 0.1% formic acid; B = LCMS grade acetonitrile with 0.1% formic acid). Fractions were collected at 30 s intervals for 35 min into acid-cleaned and methanol rinsed deep 96-well plates, concentrated for 2 h under vacuum and analyzed by LC-ESIMS (see section Siderophore Identification in Station ALOHA Seawater) to confirm the presence of each amphibactin in individual wells (Supplementary Figure 1).

Dissolved Iron and Iron-Binding Ligand Determination by Voltammetry

Dissolved Fe concentrations were determined using adsorptive cathodic stripping voltammetry (CSV) on a 663 VA Stand controlled growth mercury electrode connected to an Eco-Chemie μAutolab-III analyzer (Metrohm USA). Briefly, 100 mL of the filtered and acidified sample was UV-irradiated for 2 h using a 909 UV Digester (Metrohm USA) in acid cleaned and Milli-Q conditioned quartz tubes. The samples were then slowly neutralized to approximately pH 8 using 1 N ammonium hydroxide (Optima, Fisher Scientific) then placed in conditioned Teflon bottles along with 5 μmol L^{-1} salicylaldoxime (SA) and 100 μL of 1.5 mol L^{-1} boric acid in 0.4 N ammonium hydroxide (pH 8.2, NBS scale). Samples were equilibrated overnight (>12 h) to ensure all Fe was associated with SA before analyses, then analyzed using standard additions and triplicate

measurements using CSV as described previously (Buck et al., 2007).

Conditional stability constants of pure amphibactins, ferrioxamines B and E, as well as organic Fe-binding ligand concentrations and strengths from water column profiles, were determined using competitive ligand exchange adsorptive cathodic stripping voltammetry (CLE-ACSV) with SA as the competing ligand (Abualhaija and van den Berg, 2014). For the determination of the conditional stability constants of the isolated amphibactins, 4 L of filtered low Fe seawater was collected from 15 m depth at Station ALOHA and was UV-irradiated for 2 h in acid cleaned quartz tubes as described above. After irradiation, the seawater was slowly passed through clean Chelex-100 resin (Bio-Rad) and irradiated a second time to ensure the seawater was metal and organic-free. For each amphibactin ligand titration, 12 separate 10 mL aliquots of UV-irradiated seawater were placed in acid-cleaned and conditioned Teflon vials. Then 50 μL of 1.5 mol L^{-1} boric acid in 0.4 N ammonium hydroxide was added to each vial (final pH = 8.2, NBS scale), along with 12.5 μL SA (final concentration of 5 μmol L^{-1}). A 5 μL aliquot from the well containing the isolated amphibactin was added to each Teflon vial, along with 10 Fe additions up to 25 nmol L^{-1}. These were equilibrated overnight before being analyzed by CLE-ACSV. Purging with nitrogen has been found to decrease the sensitivity of CLE-ACSV titrations on 663 VA stand electrodes (Abualhaija and van den Berg, 2014), so each aliquot was not purged when analyzed, and the nitrogen blanket was switched off, and vials were run in triplicate. Triplicate titrations were performed for each amphibactin and analyzed using ProMCC (Omanović et al., 2015), using an optimized sensitivity and updated Fe-SA side reaction coefficients (Abualhaija and van den Berg, 2014). Ligand strengths represent the average of the triplicate titrations analyzed using the chemical speciation fitting mode in ProMCC at the 95% confidence interval. A secondary check on the approximate concentration of each amphibactin was determined by spiking the bulk *Vibrio* media extract containing amphibactins with 3 different concentrations of Fe and an internal standard and analyzing the aliquots by LC-ICPMS (see section Siderophore Identification in Station ALOHA Seawater). Concentrations determined by CLE-ACSV were within ∼1 nmol L^{-1} of the estimates made using LC-ICPMS. Organic Fe-binding ligand samples from the water column were analyzed using CLE-ACSV as described above, using 12 titration points and overnight equilibration with 5 μmol L^{-1} SA and boric acid buffer. Titrations were also interpreted using ProMCC in chemical speciation fitting mode with optimized sensitivity (Omanović et al., 2015) and solved for a single ligand class.

Siderophore Identification in Station ALOHA Seawater

Between 16–20 L of filtered seawater was pumped at 15 mL min^{-1} through a 6 mL Bond-Elut ENV column (1 g, 6 mL, Agilent Technologies) that had been cleaned with pH 2 Milli-Q (Optima HCl), rinsed with Milli-Q, and activated with distilled methanol before a final rinse with Milli-Q. Columns were wrapped in aluminum foil to prevent photochemical degradation of the concentrated organic material during sample processing. Columns were washed with three column volumes of Milli-Q and frozen at −20°C. Prior to analyses, columns were thawed and eluted with 10 mL distilled methanol into acid-cleaned 15 mL falcon tubes. The eluent was reduced in volume to ∼500–1000 μL, and divided into equal volumes. One half of the sample was spiked with 2 μL of 100 μmol L^{-1} cyanocobalamin. The other half was placed in a separate tube and both sample splits frozen at −20°C until analysis.

All samples were analyzed by liquid chromatography inductively coupled plasma mass spectrometry (LC-ICPMS) on a quadrupole ICPMS (iCap Q; Thermo Scientific) connected to a Dionex Ultimate 3000 bioinert LC (Thermo Scientific). Aliquots of the spiked and unspiked samples (with the internal standard) were analyzed on a polyetheretherketone (PEEK) LC column (2.1 × 100 mm, 3-μm particle size C_8 resin; Hamilton) and eluted using a 20-min gradient (5 to 90% B), followed by an isocratic gradient for 10 min at 90% B, a 5 min gradient from 90 to 95% B, and an isocratic gradient at 95% B for 5 min at 200 μL min^{-1} (solvent A: 5 mmol L^{-1} ammonium formate, solvent B: 5 mmol L^{-1} ammonium formate in methanol). A post-column PEEK flow splitter directed 50 μL min^{-1} of the flow into a perfluoroalkoxy micronebulizer (PFA-ST; Elemental Scientific) and a cyclonic spray chamber that was cooled to 0°C. Oxygen was added to the sample gas at a flow of 25 mL min^{-1} to prevent the formation of reduced organic compounds onto the platinum sampler and skimmer cones. Measurements were made in kinetic energy discrimination mode with a helium collision gas that was introduced at a rate of 4.2 mL min^{-1} to remove isobaric ArO^+ interferences with ^{56}Fe. Several metals were monitored, including ^{56}Fe, ^{57}Fe, and ^{59}Co at an integration time of 0.05 s each. Siderophore concentrations were determined using a four-point calibration curve using ferrioxamine E as a standard. Signals were normalized between each sample run using the peak height of ^{59}Co from the internal standard cyanocobalamin to account for matrix effects and sensitivity changes during instrument runs. Naturally occurring cyanocobalamin was not present in detectable concentrations in any of the samples.

The HPLC system was subsequently coupled to an electrospray ionization mass spectrometer (ESI-MS; Orbitrap Fusion, Thermo Scientific). The ESI-MS was equipped with a heated electrospray ionization source and was set to a capillary voltage of 3,500 V, sheath gas 12 (arbitrary units), auxiliary gas 6 units, and sweep gas 2 units, along with ion transfer tube and vaporizer pressure temperatures of 300 and 75°C. Scans were collected in high resolution (450K) positive mode, and high energy collisional dissociation (HCD). MS^2 spectra were collected on the ion trap mass analyzer by decision making tree using a targeted siderophore list (ChelomEx; Baars et al., 2014) and the most abundant masses. Ions were trapped using an isolation window of 1 *m/z* and fragmented using a collision energy of 35%.

The ESI-MS data was converted to an open source mzML format using MSconvert (Proteowizard) and processed using in house R script based on the XCMS data structure (https://cran.r-project.org/; Tautenhahn et al., 2012b). A constant time

offset was applied to align the retention time of the internal standard (cyanocobalamin; $m/z = 678$) mass peak from the ESI-MS to the ^{59}Co peak from the ICP-MS. An isotope pattern search algorithm (Boiteau et al., 2016) was used to identify potential Fe-containing compounds that matched the abundance ratio of ^{56}Fe and ^{54}Fe, appeared as coherent peaks in the scans, and also matched an ^{56}Fe peak in the ICP-MS data. Masses indicative of the apo (metal free) form were present for some siderophores. Siderophore identifications were confirmed by matching MS^2 spectra with those of the authentic standards (Tautenhahn et al., 2012a).

Particle Incubation Experiment

To investigate mechanisms of dissolved siderophore production below the euphotic zone, an incubation experiment was conducted using settling particles collected from Lagrangian style net traps (Peterson et al., 2005; Edwards et al., 2015) and water collected from the X-Niskin rosette. One hour prior to the incubation experiment, 16 trace metal clean 250 mL PC bottles were filled with Milli-Q and microwave-sterilized until boiling. The bottles were kept closed and allowed to cool to room temperature. Particles for the incubation experiment were collected over a 24-h net trap deployment at 150 m in the Station ALOHA sampling circle. Upon recovery, trapped particles were divided into 8 equal splits in acid-cleaned 500 mL HDPE bottles. In a trace metal clean van, one split was immediately added to 4 L of unfiltered 150 m trace metal clean seawater that had been collected in a clean 10 L polycarbonate (PC) carboy within 1 h of the incubation set-up, and had been kept at 15°C in the dark. After the particles had been added, the carboy was gently inverted three times to ensure an even distribution of the particles before dispensing into 250 mL bottles. The sixteen separate 250 mL PC bottles were divided into three treatments. The treatments were a no-particle control (only containing unfiltered 150 m water, denoted as Control A and B), a sterilized control (150 m seawater and particles and microwave sterilized, denoted as Sterilized Control A and B), and a particle addition treatment (denoted as + Particles A and B). Each treatment was completed in duplicate. Bottles were incubated in a Percival-style incubator at 15°C in the dark. The incubation was terminated after 3 days, and at each time point (t = 0, 1, and 3 days) an entire 250 mL sample bottle from each replicate was sacrificed. The t = 0 time-point was processed immediately after placing the remaining bottles in the incubator, and the control with no added particles was only sampled on day 3. Each bottle was sampled for flow cytometry cell counts and dissolved siderophore analyses.

RESULTS

Nutrients, Dissolved Iron, and Flow Cytometry at Station ALOHA

Depth profiles of macronutrient concentrations, *Synechococcus*, *Prochlorococcus*, heterotrophic bacteria, and photosynthetic picoeukaryote cell abundances were typical of summer conditions at Station ALOHA. Nitrate (equal to nitrate+nitrite) varied 10-fold from ∼0.1 μmol L^{-1} in surface waters, to 1 μmol L^{-1} in the nitracline at 300 m (**Figure 1**; **Table 1**). Phosphate also increased to ∼0.1 μmol L^{-1} from our detection limit in surface waters, while silicate concentrations remained relatively constant at ∼1.2 μmol L^{-1} to 400 m (**Figure 1**). Concentrations of dissolved Fe also remained relatively constant between 0.15 nmol L^{-1} (15 m) and 0.12 nmol L^{-1} (400 m), with potentially a slight decrease immediately below the deep chlorophyll maximum (DCM; 125 m), where values ranged from 0.06 nmol L^{-1} (150 m) to 0.08 nmol L^{-1} (200 m) before recovering to 0.10 nmol L^{-1} at 300 m. (**Table 1**). Flow cytometry counts also showed typical conditions at Station ALOHA, with a dominance of *Prochlorococcus* in surface waters (1.14×10^5 cell mL^{-1}, **Table 1**), as well as elevated *Synechococcus* (**Figure 1**; **Table 1**). Cell counts decreased throughout the water column, and *Prochlorococcus*, *Synechococcus,* and other phototrophic picoeukaryotes were non-detectable below 200 m (**Figure 1**). Heterotrophic bacteria were also abundant in surface waters, with numbers ranging from 2 to 6×10^5 cells mL^{-1} in the upper 125 m, and dropping to 5×10^4 cells mL^{-1} at 400 m. These cell numbers are also typical for heterotrophic bacteria at Station ALOHA during summer months (Campbell and Vaulot, 1993).

Siderophores and the Total Iron-Binding Ligand Pool

Siderophores

Siderophore abundances and distributions varied considerably with depth, despite only small changes in Fe and macronutrient concentrations (**Figure 2**). Nine different siderophores were identified in samples collected between 15 and 400 m (**Table 2**), including the hydroxamate siderophores ferrioxamine G and E (**Figure 2**). Ferrioxamine G was present in low concentrations in 6 of 7 samples (**Table 2**), and was only absent in the 200 m sample. Ferrioxamine E was identified at 15 and 125 m (the DCM), but was below the limit of detection in the other samples. The concentrations of ferrioxamines G and E ranged from 0.1 to 1.3 pmol L^{-1} and were highest in samples above 150 m. Deep samples (300 and 400 m), were characterized by a suite of amphibactins (**Figure 2**). These siderophores all have a common head group that binds Fe, and only differ in the structure of their side chains (**Figure 2B**). Amphibactins were present in higher concentrations than ferrioxamines, with concentrations ranging from 0.1 to 6 pmol L^{-1}, with the highest concentrations (6 pmol L^{-1}) observed at 300 m (**Table 2**). To confirm our compound assignments, MS^2 data was collected for ferrioxamine E, amphibactin T, S, D, and H (**Figure 3**; **Table 2**). The abundance of ions from ferrioxamine G and other amphibactins were too low to permit MS^2 data acquisition, and compound identification rests on MS and retention time data alone. Fragmentation data for ferrioxamine E showed characteristic fragments at *m/z* 537.3 and 295.2 (**Figure 3C**), corresponding to neutral losses of $C_{20}H_{45}N_{10}O_7$ and $C_{10}H_{27}N_6O_4$ and matching those of a ferrioxamine E standard. Likewise, MS^2 spectra of amphibactins T, S, D, and H also showed characteristic fragments due to common neutral losses of 218 ($C_8H_{14}N_2O_5$), 277 ($C_{10}H_{19}N_3O_6$), and 305

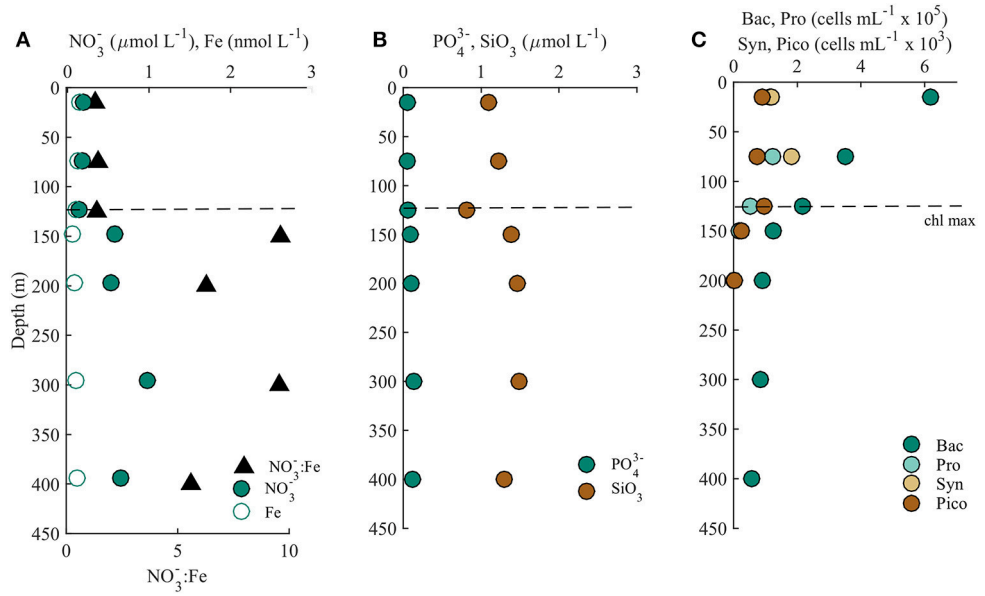

FIGURE 1 | (A) The ratio of nitrate to dissolved iron (NO_3^-:Fe, black triangles), nitrate (NO_3^-, green circles), and dissolved iron (Fe, open circles), **(B)** phosphate (PO_4^{3-}, green circles) and silicate (SiO_3), and **(C)** the distributions of heterotrophic bacteria (Bac, dark green circles), *Prochlorococcus* (Pro, light green circles), *Synechococcus* (Syn, yellow circles), and photosynthetic picoplankton (Pico, orange circles) at Station ALOHA in July 2015. The dashed line represents the location of the chlorophyll *a* maximum throughout the duration of the cruise.

TABLE 1 | Macro (nitrate, phosphate, silicate) and micro (dissolved iron) nutrient concentrations and cell counts (heterotrophic bacteria, *Prochlorococcus*, *Synechococcus*, and photosynthetic picoeukaryotes) determined from 15 to 400 m at Station ALOHA.

Depth m	Nitrate μmol L^{-1}	Phosphate μmol L^{-1}	Silicate μmol L^{-1}	Fe nmol L^{-1}	+/−	Total Bacteria cells mL^{-1}	*Prochlorococcus* cells mL^{-1}	*Synechococcus* cells mL^{-1}	Photosynthetic picoeukaryotes cells mL^{-1}
15	0.19	0.05	1.10	0.15	0.08	6.19E+05	1.14E+05	1.19E+03	8.98E+02
75	0.18	0.05	1.22	0.13	0.02	3.51E+05	1.23E+05	1.82E+03	7.39E+02
125	0.14	0.06	0.81	0.10	0.01	2.17E+05	5.26E+04	nd	9.59E+02
150	0.58	0.09	1.39	0.06	0.01	1.25E+05	1.76E+04	nd	2.48E+02
200	0.53	0.10	1.46	0.08	0.00	9.05E+04	1.35E+03	nd	2.58E+01
300	0.98	0.14	1.49	0.10	0.02	8.43E+04	nd	nd	nd
400	0.65	0.12	1.30	0.12	0.03	5.69E+04	nd	nd	nd

The "nd" notation means not determined.

($C_{11}H_{19}N_3O_7$, **Figure 3F**) as seen in previous analyses (Boiteau et al., 2016) and in the MS^2 spectra of authentic amphibactins (Supplementary Figure 2).

Our LC-ICPMS analyses measures siderophores that are bound to Fe. To measure total siderophores (both with and without Fe), 5 μmol L^{-1} of Fe was added to the sample in the form of Fe-citrate, and was left overnight to equilibrate with the Fe-free natural ligands. We observed similar concentrations of total siderophores in samples from surface depths (**Table 3**), but total siderophore concentrations in the 300 and 400 m samples increased to 11 and 3 pmol L^{-1} respectively. In addition, the uncharacterized organic matter, appearing as the unresolved baseline rise in each of the chromatograms, also increased upon the addition of Fe at each depth, signifying there is organic matter at each of our sampling depths that is under-saturated with Fe. Below 150 m, unresolved organic matter containing organic Fe-binding sites increased much more than in samples from shallower depths, indicating higher "excess" ligands in these samples. Taken together, the 300 and 400 m sample contained much higher concentrations of both siderophores and uncharacterized organic Fe-binding ligands that were under-saturated with Fe compared to upper water column samples. The total Fe-L (siderophores and unresolved baseline, **Table 3**) measured by LC-ICPMS represents about 10–30% of the total dissolved Fe (**Figure 4**; **Table 3**). A large fraction of dissolved Fe was not captured by our solid phase extraction method.

Strong Iron-Binding Organic Ligand Pool Measured by CLE-ACSV

Fe-binding organic ligands at Station ALOHA were also characterized by CLE-ACSV (**Figure 4**; **Table 3**). Using a single

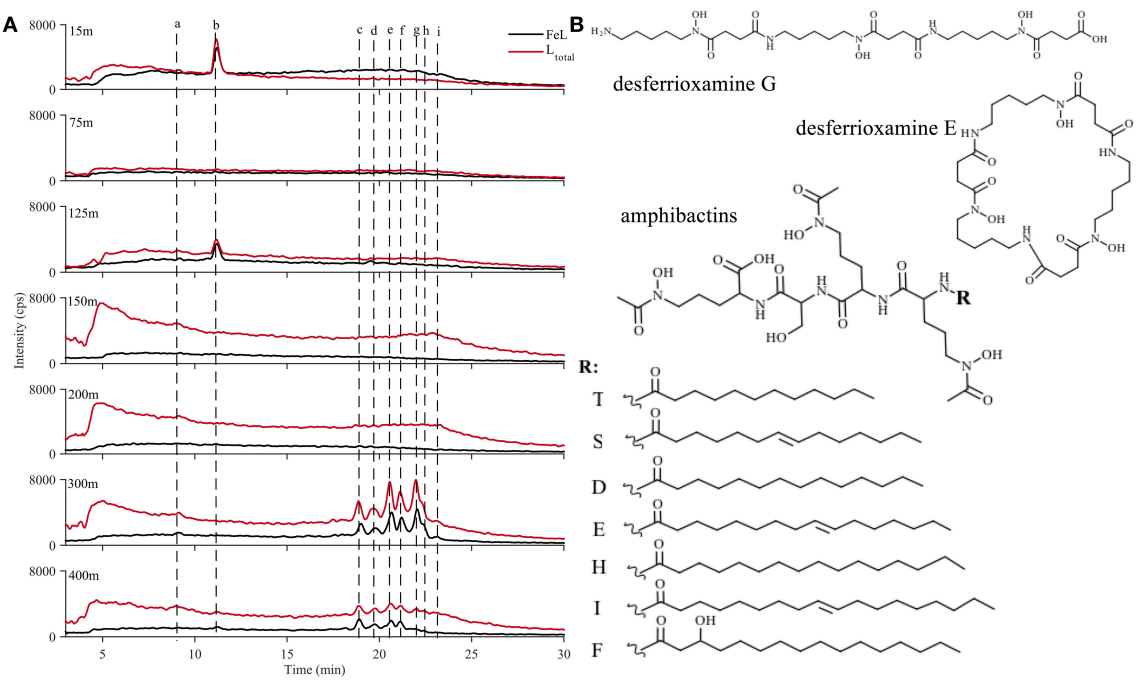

FIGURE 2 | (A) ^{56}Fe ICP-MS chromatograms from 15 m (top) to 400 m (bottom) where black represents the iron-bound ligands and red represents the total ligand concentration after an iron addition to the extract. **(B)** Structures of desferrioxamine G (peak *a*), E (peak *b*) and amphibactins (T, S, D, E, H, I, F; peaks *c–i*) identified in the water column at Station ALOHA.

TABLE 2 | Siderophore peak identities in each sample as presented in **Figure 2**, with the siderophore name, retention time (min), apo mass (iron free), ^{54}Fe and ^{56}Fe mass, and the dominant fragments from the MS^2 fragmentation spectra.

Peak	Siderophore	Retention time (min)	Apo mass	^{54}Fe mass	^{56}Fe mass	Dominant fragments
A	ferrioxamine G	9.05	619.367	670.283	672.278	nd
b	ferrioxamine E	11.07	601.356	652.272	654.268	654.39, 295.2
c	amphibactin T	18.82	804.472	855.388	857.383	552.3, 580.3
d	amphibactin S	20.34	830.488	881.404	883.399	371.2, 719.3
e	amphibactin D	20.59	832.503	883.419	885.415	580.3, 608.3
f	amphibactin E	21.11	858.519	909.435	911.430	nd
g	amphibactin H	22.01	860.534	911.450	913.445	608.3, 636.3
h	amphibactin I	22.31	874.514	925.430	927.425	nd
i	amphibactin F	22.45	876.529	927.446	929.441	490.3, 467.2

The notation "nd" means not determined. See Supplementary Figures 2–7 for fragmenetation spectra.

analytical window, one ligand class was detected at all depths. These ligands were in excess of Fe at every depth, and had a $\log K^{cond}_{FeL_1,Fe'}$ that would place them in the stronger (L_1 or L_2; $\log K^{cond}_{FeL_1,Fe'} \sim 12$) class of ligands (**Table 3**). Since volume was limited and only a single analytical window was employed, the strength of the ligands detected likely represent the average conditional stability constants of one or more ligand classes. Total Fe-binding ligands ranged from 0.9 nmol L^{-1} in surface waters to ~1.6 nmol L^{-1} at 300 and 400 m. The $\log K^{cond}_{FeL_1,Fe'}$ was relatively consistent with depth, with slightly stronger conditional stability constants in surface waters.

Conditional Stability Constants of Model Ligands

To determine the contribution of the siderophores to Fe complexation at Station ALOHA, the conditional stability constants of amphibactins T, S, D, E, and C purified from *Vibrio cyclitrophicus 1F-53* along with ferrioxamines B and E were measured using CLE-ACSV. All amphibactins had very similar conditional stability constants, ranging from 12.0 to 12.4 (**Table 4**). Ferrioxamines B and E were found to have conditional stability constants of 14.4 and 14.0 respectively, consistent with other studies ($\log K^{cond}_{FeL_1,Fe'}$ 13–14; Rue and Bruland, 1995; Witter et al., 2000).

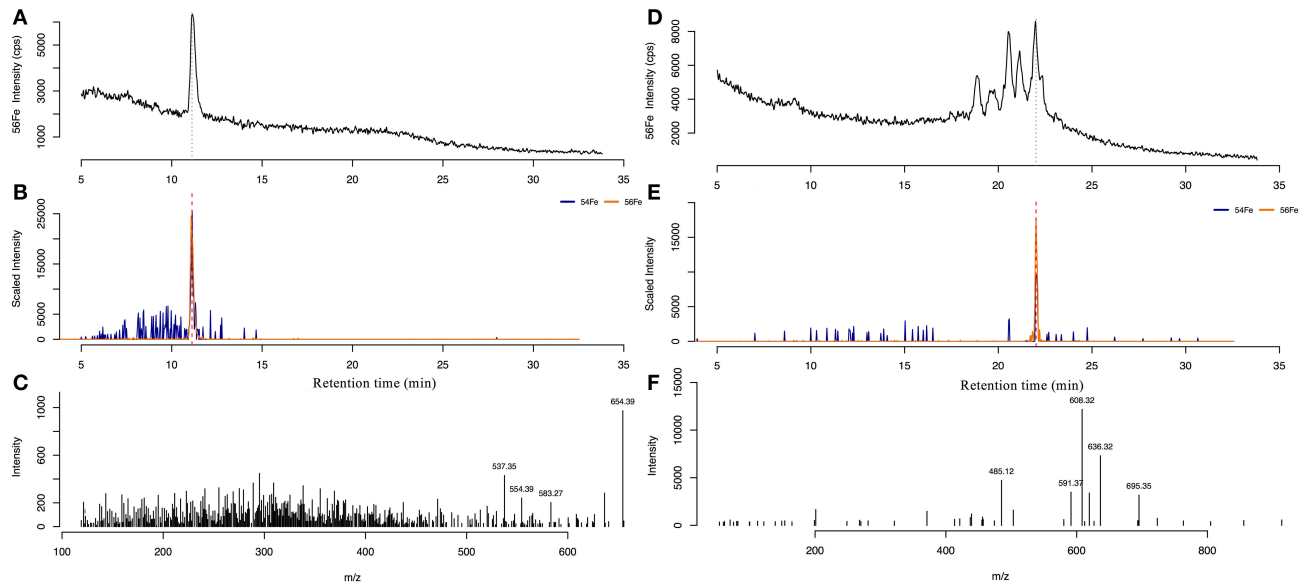

FIGURE 3 | The ^{56}Fe ICP-MS spectra (top) of ferrioxamine E **(A)** in the 15 m sample, and amphibactin H in the 300 m sample **(D)**. **(B,E)** shows the extracted ion chromatogram (EIC) of the ^{54}Fe and ^{56}Fe isotope peaks of ferrioxamine E and amphibactin H, respectively. Bottom panels show the MS^2 fragmentation spectra from the compound at the corresponding retention time for ferrioxamine E **(C)** and amphibactin H **(F)**.

TABLE 3 | Siderophore and total iron binding ligand parameters determined at Station ALOHA.

Depth m	Fe nmol L^{-1}	L nmol L^{-1}	logK	Fe' pmol L^{-1}	FeL pmol L^{-1}	Fe(Ferrioxamine) pmol L^{-1}	Fe(Amphibactin) pmol L^{-1}	Ferrioxamine Total pmol L^{-1}	Amphibactin Total pmol L^{-1}
15	0.15	0.88	12.44	0.07	41.73	1.35	0.16	2.16	0.27
75	0.13	0.90	12.19	0.11	13.53	0.03	0.17	0.06	0.20
125	0.10	0.96	12.00	0.12	21.00	0.86	0.77	0.92	0.77
150	0.06	1.61	11.89	0.05	12.66	0.04	0.15	0.07	0.15
200	0.08	1.41	11.90	0.08	12.98	nd	0.65	nd	0.83
300	0.10	1.57	11.93	0.08	23.29	1.20	6.30	1.20	11.05
400	0.12	1.55	11.76	0.14	12.46	0.13	2.60	0.13	2.96

Dissolved iron (Fe), total iron-binding ligands (L), and conditional stability constants (logK) were determined using cathodic stripping voltammetry, and Fe' (inorganic Fe) was calculated by $Fe' = Fe/[(L - Fe) \times K]$. Siderophore parameters were determined using LC-ICPMS and include a calculation of total iron-binding ligands (FeL; measured as the area under the chromatographic curve in ICP-MS analyses), iron bound to ferrioxamine-type siderophores [Fe(Ferrioxamine)], iron bound to amphibactins-type siderophores [Fe(Amphibactin)], as well as the total concentration of ferrioxamines (Ferrioxamine Total) and amphibactins (Amphibactin Total) after adding Fe to the sample and analyzing again by LC-ICPMS. The notation "nd" refers to not determined.

Siderophore Production During Particle Regeneration Incubations

To assess the potential contribution of particle regeneration to the high concentrations of siderophores measured at 300 and 400 m, we measured siderophore production from particle-associated bacteria during organic matter regeneration of sinking particles (**Figure 5**). Very low concentrations of siderophores were observed in the water column at 150 m, just below the DCM (**Figure 2**), and in all treatments at the beginning of the particle incubation experiments (**Figure 5A**; t = 0). The only siderophore detected in the initial conditions of the incubation with no particles added was ferrioxamine E (0.02 pmol L^{-1}). After 1 day, significantly higher concentrations of ferrioxamine E (0.4 pmol L^{-1}, *t*-test, $p < 0.05$) were detected in the particle amended treatment, but not in the non-amended or sterilized controls (**Figure 5A**). After 3 days, concentrations of ferrioxamine E had not changed in the controls of sterilized treatments, while concentrations in the +Particles treatments remained high, within the range observed on day 1 (**Figure 5A**). The production of ferrioxamine E in +Particle treatments was also accompanied by an increase in heterotrophic bacteria compared to control treatments (**Figure 5B**). However, no amphibactins were observed in the experiment.

DISCUSSION

Siderophores at Station ALOHA

Dissolved Fe concentrations in the upper water column (<500 m) at Station ALOHA are generally low (0.1–0.5 nmol L^{-1}; Fitzsimmons et al., 2015), but not limiting (Boyle et al., 2005).

At the time of our sampling, dissolved Fe concentrations were >0.06 nmol L^{-1}, but nevertheless siderophores were present at several depths between 5 and 400 m, with strikingly different distributions in the upper and lower portions of our profile. Ferrioxamine E was by far the most abundant siderophore in the euphotic zone, with picomolar concentrations in the surface (15 m) and in the DCM (125 m). We found small amounts of ferrioxamine G at these depths as well. Both ferrioxamine E and G have been found to be produced by the marine heterotroph *Pseudomonas* spp. (Meyer and Abdallah, 1980; Essén et al., 2007), and ferrioxamine G has been identified in cultures of marine *Vibrio* species (Martinez et al., 2001). Ferrioxamines have also been observed in the Atlantic (Mawji et al., 2008), and the coastal Pacific (Boiteau et al., 2016). Summertime rates of primary production and nitrogen fixation at Station ALOHA are highest in the surface mixed layer (<50 m; Karl and Church, 2014; Böttjer et al., 2017), where microbial Fe demand would be expected to reach a maximum as well. Nitrogen fixing cyanobacteria such as *Trichodesmium* and diatoms (*Hemiaulus, Rhizoselenia*), hosting endosymbiotic diazotrophs (*Richelia*), are common in the upper water column in summer (Karl et al., 2012), and may experience Fe stress due to their higher Fe requirements and larger cell sizes. A large fraction of Fe in ALOHA surface waters is supplied by the deposition of atmospheric dust, which may include Fe in a mineral form (Boyle et al., 2005; Fitzsimmons et al., 2015). Ferrioxamines have very strong stability constants ($\log K^{cond}_{FeL_1,Fe'} >$ 14), and have been shown to be particularly effective at dissolving Fe minerals (Akafia et al., 2014). Ferrioxamines E and G have also been reported in surface waters of the oligotrophic North Atlantic Ocean (Mawji et al., 2008), a region with moderately high concentrations of Fe largely sourced from atmospheric dust (Jickells et al., 2005; Mahowald et al., 2005; Conway and John, 2014) that supports abundant *Trichodesmium* spp. and *Richelia*-diatom nitrogen fixers. Heterotrophic bacteria associated with these nitrogen-fixing cyanobacteria are an additional possible source of ferrioxamines at Station ALOHA, and perhaps at other oligotrophic sites where *Trichodesmium* and diatom-diazotroph associations are abundant, however direct evidence of siderophore production from these assemblages has not been observed.

Rates of primary production and nitrogen fixation fall rapidly between 15 and 75 m (Karl and Church, 2014; Böttjer et al., 2017), while Fe concentrations remain relatively stable (∼0.1 nmol L^{-1}). Only trace amounts of ferrioxamine G were detected in our 75 m sample, suggesting depth dependent changes in bacteria species, microbial activity or Fe concentrations that may decrease Fe stress. It is possible the bacteria responsible for producing siderophores were absent at 75 m, or perhaps the combination of sufficient dissolved Fe and low(er) rates of primary productivity and nitrogen fixation, may have reduced the demand for Fe at 75 m, making the synthesis of siderophores unnecessary. Using similar reasoning, even though Fe concentrations were at a minimum (0.06–0.08 nmol L^{-1}) in the 150 and 200 m samples, the number of bacterial cells, particularly photoautotrophs, falls rapidly below 125 m (**Figure 1**). The near absence of siderophores between 150 and 200 m may indicate a decrease in Fe demand, or Fe stress overall, within the community.

The highest concentration of siderophores in our profile was found at 300 m, where we detected a suite of seven amphibactins. Amphibactins are hybrid compounds composed of a peptidic, Fe-complexing portion, and a lipid portion that allows these siderophores to form strong associations with cell membranes (reviewed in Vraspir and Butler, 2009). These membrane associations may reduce diffusive loss of amphibactins to the environment, creating a more favorable energy balance between Fe uptake and loss of siderophore to the environment. Although dissolved Fe concentrations between 300 and 400 m were ∼0.1 nmol L^{-1}, nearly half the amphibactins in both samples were not complexed to Fe. Addition of Fe to our 300 m sample increased the total Fe-amphibactin by ∼45%, from ∼6 to ∼11 pmol L^{-1}. Total amphibactin concentrations at depth at ALOHA were similar to the values reported for surface waters of the HNLC eastern tropical Pacific Ocean (Boiteau et al., 2016).

Amphibactins at 300 m were most likely produced at depth, and not passively introduced from the regeneration of sinking particles or laterally from advection. Amphibactins were not detected in any samples collected above 300 m. Shipboard incubations of sinking particles collected in sediment traps only yielded small amounts of ferrioxamine E, but no amphibactins were produced. Although the time scales of amphibactin cycling at 300 m may integrate longer periods than captured by our euphotic zone sampling and particle incubation experiments, we found no evidence of amphibactin production in the euphotic zone and subsequent transport to depth. Therefore, we inferred that amphibactins were synthesized by bacteria at 300 and 400 m. Such high concentrations of amphibactins in the mesopelagic were surprising. Although there is some evidence for Fe limitation of heterotrophic production in surface waters of the Southern Ocean (Church et al., 2000), low rates of bacterial production coupled to high dissolved Fe concentrations characteristic of meso- and bathypelagic regions were not expected to induce production of siderophores in higher concentrations than in the euphotic zone.

We note that at Station ALOHA, water between 300 and 400 m forms the upper portion of the North Pacific Intermediate Water (NPIW) salinity minimum, which outcrops in the low Fe region of the northwest subpolar gyre (Talley, 1993). Concentrations of dissolved Fe transported with NPIW are expected to be low, and bioavailable Fe may represent only a fraction of the total dissolved Fe. Low Fe bioavailability may be one factor inducing Fe stress within the 300–400 m zone. We expected that much of the bioavailable Fe in the 300–400 m region was supplied from remineralization of Fe-containing proteins in sinking particulate organic matter. Some Fe from this sinking organic matter is bound by the ∼1.5 nmol L^{-1} strong ligands measured by CLE-ACSV (discussed in the next section). Amphibactins have conditional stability constants that are much weaker than ferrioxamines, but are nevertheless strong enough to compete with the other organic ligands for some portion of the dissolved Fe. The distinct sources of Fe from dust and sinking particles to the upper and lower regions of the Station ALOHA water column

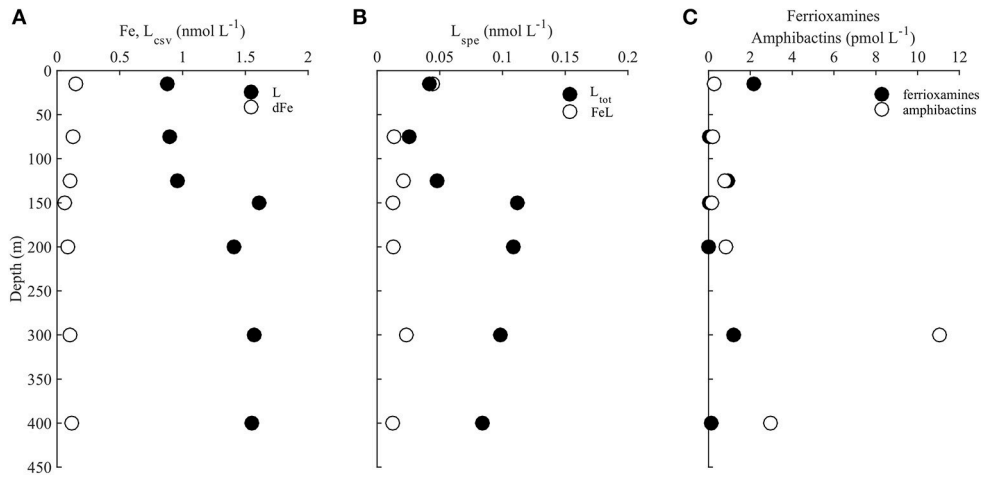

FIGURE 4 | (A) Dissolved iron (Fe, open circles) and total ligands determined using electrochemical methods (L_{CSV}, black circles), **(B)** iron-bound ligands (FeL, open circles) and total ligands (L_{tot}, black circles) determined by solid phase extraction, **(C)** and total concentrations (iron bound and excess) of ferrioxamines (ferrioxamine G+E, black circles) and amphibactins (amphibactins T+S+D+E+H+I+F, open circles) throughout the water column at station ALOHA.

TABLE 4 | Conditional stability constants (logK) of isolated amphibactins from *Vibrio cyclitrophicus 1F-53*, as well as model siderophores ferrioxamine E and B.

Ligand	logK	+/−
amphibactin T	12.40	0.03
amphibactin S	12.48	0.07
amphibactin D	12.07	0.15
amphibactin E	12.06	0.08
amphibactin C*	12.00	0.03
ferrioxamine E	14.05	0.09
ferrioxamine B**	14.42	0.08

Amphibactin C was not observed in the water column, but was effectively isolated from Vibrio cyclitrophicus 1F-53.

**Ferrioxamine B was not observed in the water column, but was used as a model siderophore for ferrioxamine G.*

may influence the types of siderophores microbes produce in and below the euphotic zone.

Comparison of Ligand Distribution Determined by CLE-ACSV and Siderophores Measured by LC-ICPMS

Efforts to model Fe cycling and bioavailability have largely focused on parameterizing the distribution of strong Fe-binding ligands (L_1) measured by CLE-ACSV (Tagliabue et al., 2014, 2016, 2017). It has long been assumed that siderophores are a component of L_1 (Gledhill and Buck, 2012). However, no direct comparisons of siderophore and L_1 concentrations have been made. In this study we used CLE-ACSV with a single analytical window rather than the multiple windows used in some other studies (Bundy et al., 2014, 2015, 2016; Hogle et al., 2016a). Thus, the ligands measured here likely represent an average of the very strong (L_1; $\log K^{cond}_{FeL_1,Fe'} > 12$) and relatively strong (L_2; $\log K^{cond}_{FeL_1,Fe'} < 12$) ligands measured by others (Gledhill and Buck, 2012; Bundy et al., 2014, 2016; Hogle et al., 2016a). Both L_1 and L_2 are considered to be "strong" Fe-binding ligands, thus we will refer to the ligands characterized by our measurements as strong ligands.

Beyond simply comparing their distributions, there are two important considerations for determining whether or not the siderophores are detected as strong ligands by voltammetry. The first is to consider whether or not siderophores fall within the analytical window of CLE-ACSV. The analytical window of the voltammetric measurements is defined by α'_{CL}, which is the side reaction coefficient of the competitive ligand (CL) used in the measurements. The side reaction coefficient is defined by,

$$\alpha'_L = [L'] \times K^{cond}_{FeL,Fe'} \quad (1)$$

where α'_L represents the side reaction coefficient of the ligand (L) being considered, $[L']$ is the concentration of the free ligand, and $K^{cond}_{FeL,Fe'}$ is the conditional stability constant (binding strength to Fe). If α'_L is greater than or less than 10 times that of the competing ligand (α'_{CL}) then the detection of that particular ligand (in this case, the siderophore) is outside of the analytical window of the voltammetric measurement (van den Berg and Donat, 1992). We used salicylaldoxime (SA) as the competing ligand in our analyses, which has $\alpha'_{SA} = 17.9$. The $\alpha'_{ferrioxamine}$ is ~200, more than 10 times α'_{SA}. The ferrioxamines we measured at Station ALOHA by ICP-MS therefore, likely do not contribute to the concentration of L determined by voltammetry. However, the $\alpha'_{amphibactins}$ do fall within the range of the analytical window used, so our measurement of L likely includes a contribution from amphibactins.

The second important aspect that determines whether or not siderophores were captured in the voltammetric measurements is the kinetics of Fe exchange. Since the majority of the ferrioxamines, as well as a portion of the amphibactins detected in this profile were bound to Fe (**Figure 2**), it is possible the

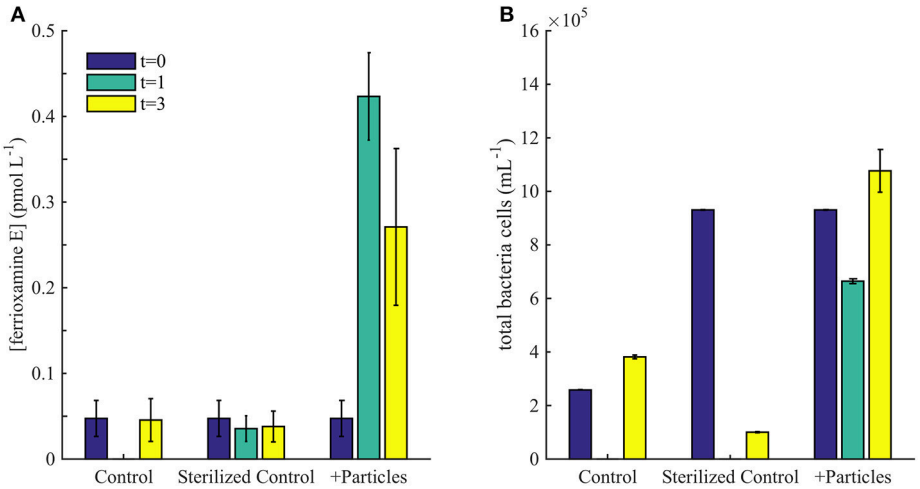

FIGURE 5 | (A) Concentrations of ferrioxamine E observed in particle incubation experiment on day 0, 1, and 3. **(B)** Flow cytometry cell counts during the incubation experiment.

natural Fe bound to these compounds did not exchange with the added Fe in the voltammetry titrations. If no exchange occurs, those ligands will not be detected as a separate and distinct ligand class by voltammetry (Gledhill and Buck, 2012), but will be accounted for in the average ligand parameters. Laboratory experiments of ^{56}Fe:^{57}Fe exchange between ferrioxamine E and natural organic ligands in seawater suggest very slow exchange kinetics (Boiteau, 2016). Coupled to the high value of $\alpha'_{ferrioxamine}$, our voltammetric measurements largely missed any contribution of ferrioxamines to the total L pool. Fe exchange kinetics for amphibactins are somewhat faster, but are still slow relative to the equilibration times used in our measurements (Boiteau, 2016). This exchange reaction may be accelerated to some extent in the presence of high concentrations of SA used in the titration via an associative mechanism. Our voltammetric measurements therefore likely captured ∼45% of apo-amphibactins at depth, and a small fraction of Fe-amphibactins. Despite the encouraging coherence between the concentration profiles of siderophores and L measured by voltammetry (**Figures 4A,B**), the ligand pools measured by these two methods only partially overlap. Many Fe-siderophores are likely missed by traditional voltammetric techniques (Hawkes et al., 2013), while LC-ICPMS only measures the fraction of ligands captured by solid phase extraction.

Estimating the Contribution of Siderophores to Iron Cycling at Station ALOHA

Previous work at Station ALOHA has shown that Fe varies seasonally and interannually in the upper 250 m, and that organic Fe-binding ligands often vary along with dissolved Fe with a time lag on the order of days (Fitzsimmons et al., 2015). The covariation in dissolved Fe and ligands suggests a dynamic interaction between Fe and organic ligand production, as well as active mediation of Fe cycling by the microbial community (Adly et al., 2015). To estimate the potential availability of siderophore bound Fe, we compared their concentration to inorganic Fe (Fe') which is thought to be the most bioavailable form of Fe (**Table 3**; Shaked et al., 2005; Shaked and Lis, 2012; Lis et al., 2015).

In order to determine the relative contribution of siderophore bound Fe, Fe', and FeL to total dissolved Fe, we can consider the equilibrium Fe speciation at Station ALOHA in our profile using the following relationship,

$$K^{cond}_{FeL,Fe'} = \frac{[FeL]}{[Fe'][L']} \quad (2)$$

From this equation and values of L and K determined by voltammetry, we can calculate the distribution of Fe' and compare that to the concentration of Fe bound by siderophores determined by ICP-MS in order to infer the relative importance of these species in biological Fe uptake. The amount of Fe bound to siderophores at 15 m is twice as high as inorganic Fe (Fe'; **Table 3**). However, at 300 m siderophore-bound Fe is approximately two orders of magnitude higher (∼10 pmol L^{-1}) than inorganic Fe concentrations (0.1 pmol L^{-1}; Shaked et al., 2005; Shaked and Lis, 2012; Lis et al., 2015). Even at the lower concentrations of siderophores present in surface waters (0.1–2 pmol L^{-1}), Fe-siderophore concentrations are still greater than Fe' due to the stronger conditional stability constants determined at these depths (**Table 3**). Fe bound to unknown ligands (L) in the chemical speciation calculations represent the vast majority (99%) of the dissolved Fe. Although Fe' is thought to be the most bioavailable form of Fe (Lis et al., 2015), the very low concentrations of Fe' present in seawater suggest that organic pools of Fe are very important. Based on data from phytoplankton Fe uptake experiments (Lis et al., 2015), we can infer that on average, FeL is taken up by phytoplankton at 1–10% the rate of Fe' uptake, while FeL concentrations are >100 greater than Fe' concentrations (**Table 3**).

Dynamic Iron Cycling at Station ALOHA

The presence of siderophores in the upper water column indicates that even though Fe is not thought to be limiting at Station ALOHA, some populations of microbes are likely responding to Fe stress, perhaps in response to low Fe concentrations and high biological demand. Biological responses to low Fe are not unprecedented at our study site, and have been observed in surface waters due to dust events or passing mesoscale eddies that contain elevated Fe (Fitzsimmons et al., 2015). Our results show that the microbial response to low Fe was not uniform throughout the Station ALOHA water column. Siderophore concentrations and types changed rapidly with depth. If Fe stress arises from a combination of Fe bioavailability, concentration, and microbial Fe demand, the rapidly changing profile of siderophores at Station ALOHA suggests these factors are dynamic, and at least vertically, can change over spatial scales of only a few tens of meters. The two major classes of siderophores we observed, ferrioxamines and amphibactins, have strikingly different conditional stability constants and abilities to form associations with cell membranes. Their distribution in the water column could be due to many factors, but it may reflect subtle differences in the nature of Fe available for complexation.

Dynamic responses to Fe have primarily been observed in surface waters, and the effects of Fe on mesopelagic communities have been relatively understudied. The high concentrations of siderophores between 300 and 400 m, as well as the rapid production of ferrioxamine E in our particle incubation experiment at a rate of 0.08 pmol L^{-1} day^{-1} (**Figure 5**), indicate that Fe bioavailability is a factor in organic matter degradation below the euphotic zone. Our incubation results confirm results from other studies (Boyd et al., 2010; Bundy et al., 2016; Velasquez et al., 2016), and demonstrate that siderophores are produced by bacteria associated with sinking particles. Sinking particles are a microenvironment where macronutrients are elevated, but Fe could be in forms that are not readily available (Hogle et al., 2016b). It was surprising that no amphibactins were produced in our experiment, however it may be that the short duration of the incubation favored fast-growing, copiotrophic bacteria that produce ferrioxamines (Cordero et al., 2012). Regardless, the high concentrations of siderophores in this profile, as well as the strong ligands observed in voltammetry studies throughout the deep ocean (Buck et al., 2015; Gerringa et al., 2015) suggests that bacteria are actively interacting with Fe on sinking particles during the regeneration processes.

AUTHOR CONTRIBUTIONS

RaB was responsible for sample collection, experimental design, sample analyses, and data interpretation. ReB and CM isolated amphibactins from culture and contributed to data acquisition and analyses. KT-K analyzed flow cytometry samples. BV helped design and implement the sediment trap collections and particle incubation experiments. MM assisted with mass spectral data analyses. MS and DR contributed to experimental design, analyses, and data interpretation. RaB wrote the paper with assistance from all coauthors.

ACKNOWLEDGMENTS

We thank Chief Scientists Tara Clemente and Sam Wilson for leading the SCOPE Diel cruises. We also thank the Captain and crew of the R/V *Ka'imikai-O-Kanaloa*, as well as Paul Henderson in the Woods Hole Oceanographic Nutrient Analytical Facility for nutrient analyses. This work was funded by the Woods Hole Oceanographic Postdoctoral Fellowship for RaB, the Simons Foundation (Award 329108), and the National Science Foundation (OCE-1356747). We also thank two reviewers for helpful comments on the manuscript.

SUPPLEMENTARY MATERIAL

The Supplementary Material for this article can be found online at: https://www.frontiersin.org/articles/10.3389/fmars.2018.00061/full#supplementary-material

REFERENCES

Abualhaija, M. M., and van den Berg, C. M. (2014). Chemical speciation of iron in seawater using catalytic cathodic stripping voltammetry with ligand competition against salicylaldoxime. *Mar. Chem.* 164, 60–74. doi: 10.1016/j.marchem.2014.06.005

Adly, C. L., Tremblay, J. E., Powell, R. T., Armstrong, E., Peers, G., and Price, N. M. (2015). Response of heterotrophic bacteria in a mesoscale iron enrichment in the northeast subarctic Pacific Ocean. *Limnol. Oceanogr.* 60, 136–148. doi: 10.1002/lno.10013

Akafia, M. M., Harrington, J. M., Bargar, J. R., and Duckworth, O. W. (2014). Metal oxyhydroxide dissolution as promoted by structurally diverse siderophores and oxalate. *Geochim. Cosmochim. Acta* 141, 258–269. doi: 10.1016/j.gca.2014.06.024

Baars, O., Morel, F. M., and Perlman, D. H. (2014). ChelomEx: isotope-assisted discovery of metal chelates in complex media using high-resolution LC-MS. *Anal. Chem.* 86, 11298–11305. doi: 10.1021/ac503000e

Berman-Frank, I., Cullen, J. T., Shaked, Y., Sherrell, R. M., and Falkowski, P. G. (2001). Iron availability, cellular iron quotas, and nitrogen fixation in Trichodesmium. *Limnol. Oceanogr.* 46, 1249–1260. doi: 10.4319/lo.2001.46.6.1249

Boiteau, R. M. (2016). *Molecular Determination of Marine Iron Ligands by Mass Spectrometry*. Doctoral dissertation, Massachusetts Institute of Technology.

Boiteau, R. M., Fitzsimmons, J. N., Repeta, D. J., and Boyle, E. A. (2013). Detection of iron ligands in seawater and marine cyanobacteria cultures by high-performance liquid chromatography-inductively coupled plasma-mass spectrometry. *Anal. Chem.* 85, 4357–4362. doi: 10.1021/ac3034568

Boiteau, R. M., Mende, D. R., Hawco, N. J., McIlvin, M. R., Fitzsimmons, J. N., Saito, M. A., et al. (2016). Siderophore-based microbial adaptations to iron scarcity across the eastern Pacific Ocean. *Proc. Natl. Acad. Sci. U.S.A.* 113, 14237–14242. doi: 10.1073/pnas.1608594113

Boiteau, R. M., and Repeta, D. J. (2015). An extended siderophore suite from *Synechococcus* sp PCC 7002 revealed by LC-ICPMS-ESIMS. *Metallomics* 7, 877–884. doi: 10.1039/C5MT00005J

Böttjer, D., Dore, J. E., Karl, D. M., Letelier, R. M., Mahaffey, C., Wilson, S. T., et al. (2017). Temporal variability of nitrogen fixation and particulate nitrogen export at Station ALOHA. *Limnol. Oceanogr.* 62, 200–216. doi: 10.1002/lno.10386

Boyd, P. W., and Ellwood, M. J. (2010). The biogeochemical cycle of iron in the ocean. *Nat. Geosci.* 3, 675–682. doi: 10.1038/ngeo964

Boyd, P. W., Ibisanmi, E., Sander, S. G., Hunter, K. A., and Jackson, G. A. (2010). Remineralization of upper ocean particles: implications for iron biogeochemistry. *Limnol. Oceanogr.* 55, 1271–1288. doi: 10.4319/lo.2010.55.3.1271

Boye, M., Aldrich, A., van den Berg, C. M. G., de Jong, J. T. M., Nirmaier, H., Veldhuis, M., et al. (2006). The chemical speciation of iron in the north-east Atlantic Ocean. *Deep Sea Res. Part I Oceanogr. Res. Pap.* 53, 667–683. doi: 10.1016/j.dsr.2005.12.015

Boye, M., van den Berg, C. M. G., de Jong, J. T. M., Leach, H., Croot, P., and de Baar, H. J. W. (2001). Organic complexation of iron in the Southern Ocean. *Deep Sea Res. Part I Oceanogr. Res. Pap.* 48, 1477–1497. doi: 10.1016/S0967-0637(00)00099-6

Boyle, E. A., Bergquist, B. A., Kayser, R. A., and Mahowald, N. (2005). Iron, manganese, and lead at hawaii ocean time-series station ALOHA: temporal variability and an intermediate water hydrothermal plume. *Geochim. Cosmochim. Acta.* 69, 933–952. doi: 10.1016/j.gca.2004.07.034

Buck, K. N., and Bruland, K. W. (2007). The physicochemical speciation of dissolved iron in the Bering Sea, Alaska. *Limnol. Oceanogr.* 52, 1800–1808. doi: 10.4319/lo.2007.52.5.1800

Buck, K. N., Lohan, M. C., Berger, C. J. M., and Bruland, K. W. (2007). Dissolved iron speciation in two distinct river plumes and an estuary: implications for riverine iron supply. *Limnol. Oceanogr.* 52, 843–855. doi: 10.4319/lo.2007.52.2.0843

Buck, K. N., Sedwick, P. N., Sohst, B., and Carlson, C. A. (in press). Organic complexation of iron in the eastern tropical South Pacific: results from US GEOTRACES Eastern Pacific Zonal Transect (GEOTRACES cruise GP16). *Mar. Chem.* doi: 10.1016/j.marchem.2017.11.007

Buck, K. N., Selph, K. E., and Barbeau, K. A. (2010). Iron-binding ligand production and copper speciation in an incubation experiment of Antarctic Peninsula shelf waters from the Bransfield Strait, Southern Ocean. *Mar. Chem.* 122, 148–159. doi: 10.1016/j.marchem.2010.06.002

Buck, K. N., Sohst, B., and Sedwick, P. N. (2015). The organic complexation of dissolved iron along the US GEOTRACES (GA03) North Atlantic Section. *Deep Sea Res. Part II Top. Stud. Oceanogr.* 116, 152–165. doi: 10.1016/j.dsr2.2014.11.016

Bundy, R. M., Abdulla, H. A. N., Hatcher, P. G., Biller, D. V., Buck, K. N., and Barbeau, K. A. (2015). Iron-binding ligands and humic substances in the San Francisco Bay estuary and estuarine-influenced shelf regions of coastal California. *Mar. Chem.* 173, 183–194. doi: 10.1016/j.marchem.2014.11.005

Bundy, R. M., Biller, D. V., Buck, K. N., Bruland, K. W., and Barbeau, K. A. (2014). Distinct pools of dissolved iron-binding ligands in the surface and benthic boundary layer of the California Current. *Limnol. Oceanogr.* 59, 769–787. doi: 10.4319/lo.2014.59.3.0769

Bundy, R. M., Jiang, M., Carter, M., and Barbeau, K. (2016). A. Iron-binding ligands in the southern California current system: mechanistic studies. *Front. Mar. Sci.* 3:27. doi: 10.3389/fmars.2016.00027

Butler, A. (1998). Acquisition and utilization of transition metal ions by marine organisms. *Science* 281, 207–210. doi: 10.1126/science.281.5374.207

Butler, A. (2005). Marine siderophores and microbial iron mobilization. *Biometals* 18, 369–374. doi: 10.1007/s10534-005-3711-0

Campbell, L., and Vaulot, D. (1993). Photosynthetic picoplankton community structure in the subtropical North Pacific Ocean near Hawaii (station ALOHA). *Deep Sea Res. Part I Oceanogr. Res. Pap.* 40, 2043–2060. doi: 10.1016/0967-0637(93)90044-4

Church, M. J., Hutchins, D. A., and Ducklow, H. W. (2000). Limitation of bacterial growth by dissolved organic matter and iron in the Southern Ocean. *Appl. Environ. Microbiol.* 66, 455–466. doi: 10.1128/AEM.66.2.455-466.2000

Conway, T. M., and John, S. G. (2014). Quantification of dissolved iron sources to the North Atlantic Ocean. *Nature* 511, 212–215. doi: 10.1038/nature13482

Cordero, O. X., Ventouras, L. A., DeLong, E. F., and Polz, M. F. (2012). Public good dynamics drive evolution of iron acquisition strategies in natural bacterioplankton populations. *Proc. Natl. Acad. Sci. U.S.A.* 109, 20059–20064. doi: 10.1073/pnas.1213344109

Croot, P. L., Andersson, K., Ozturk, M., and Turner, D. R. (2004). The distribution and specification of iron along 6 degrees E in the Southern Ocean. *Deep Sea Res. Part II Top. Stud. Oceanogr.* 51, 2857–2879. doi: 10.1016/j.dsr2.2003.10.012

Edwards, B. R., Bidle, K. D., and Van Mooy, B. A. (2015). Dose dependent regulation of microbial activity on sinking particles by polyunsaturated aldehydes: implications for the carbon cycle. *Proc. Natl. Acad. Sci. U.S.A.* 112, 5909–5914. doi: 10.1073/pnas.1422664112

Essén, S. A., Johnsson, A., Bylund, D., Pedersen, K., and Lundström, U. S. (2007). Siderophore production by *Pseudomonas stutzeri* under aerobic and anaerobic conditions. *Appl. Environ. Microbiol.* 73, 5857–5864. doi: 10.1128/AEM.00072-07

Fitzsimmons, J. N., Hayes, C. T., Al-Subiai, S. N., Zhang, R., Morton, P. L., Weisend, R. E., et al. (2015). Daily to decadal variability of size-fractionated iron and iron-binding ligands at the Hawaii Ocean time-series station ALOHA. *Geochim. Cosmochim. Acta* 171, 303–324. doi: 10.1016/j.gca.2015.08.012

Gerringa, L. J. A., Blain, S., Laan, P., Sarthou, G., Veldhuis, M. J. W., Brussaard, C. P. D., et al. (2008). Fe-binding dissolved organic ligands near the Kerguelen Archipelago in the Southern Ocean (Indian sector). *Deep Sea Res. Part II Top. Stud. Oceanogr.* 55, 5–7. doi: 10.1016/j.dsr2.2007.12.007

Gerringa, L. J. A., Veldhuis, M. J. W., Timmermans, K. R., Sarthou, G., and de Baar, H. J. W. (2006). Co-variance of dissolved Fe-binding ligands with phytoplankton characteristics in the Canary Basin. *Mar. Chem.* 102, 276–290. doi: 10.1016/j.marchem.2006.05.004

Gerringa, L., Rijkenberg, M., Schoemann, V., Laan, P., and de Baar, H. (2015). Organic complexation of iron in the West Atlantic Ocean. *Mar. Chem.* 177, 434–446. doi: 10.1016/j.marchem.2015.04.007

Gledhill, M., and Buck, K. N. (2012). The organic complexation of iron in the marine environment: a review. *Front. Microbiol.* 3:69. doi: 10.3389/fmicb.2012.00069

Gledhill, M., McCormack, P., Ussher, S., Achterberg, E. P., Mantoura, R. F. C., and Worsfold, P. J. (2004). Production of siderophore type chelates by mixed bacterioplankton populations in nutrient enriched seawater incubations. *Mar. Chem.* 88, 75–83. doi: 10.1016/j.marchem.2004.03.003

Hawkes, J. A., Gledhill, M., Connelly, D. P., and Achterberg, E. P. (2013). Characterisation of iron binding ligands in seawater by reverse titration. *Anal. Chim. Acta* 766, 53–60. doi: 10.1016/j.aca.2012.12.048

Haygood, M. G., Holt, P. D., and Butler, A. (1993). Aerobactin production by a planktonic marine vibrio sp. *Limnol. Oceanogr.* 38, 1091–1097. doi: 10.4319/lo.1993.38.5.1091

Hogle, S. L., Bundy, R. M., Blanton, J. M., Allen, E. E., and Barbeau, K. A. (2016a). Copiotrophic marine bacteria are associated with strong iron-binding ligand production during phytoplankton blooms. *Limnol. Oceanogr. Lett.* 1, 36–43. doi: 10.1002/lol2.10026

Hogle, S. L., Thrash, J. C., Dupont, C. L., and Barbeau, K. A. (2016b). Trace metal acquisition by marine heterotrophic bacterioplankton with contrasting trophic strategies. *Appl. Environ. Microbiol.* 82, 1613–1624. doi: 10.1128/AEM.03128-15

Holm-Hansen, O., Kahru, M., and Hewes, C. D. (2005). Deep chlorophyll a maxima (DCMs) in pelagic Antarctic waters. II. Relation to bathymetric features and dissolved iron concentrations. *Mar. Ecol. Prog. Ser.* 297, 71–81. doi: 10.3354/meps297071

Hopkinson, B. M., and Barbeau, K. A. (2008). Interactive influences of iron and light limitation on phytoplankton at subsurface chlorophyll maxima in the eastern North Pacific. *Limnol. Oceanogr.* 53, 1303–1318. doi: 10.4319/lo.2008.53.4.1303

Hopkinson, B. M., Mitchell, B. G., Reynolds, R. A., Wang, H., Selph, K. E., Measures, C. I., et al. (2007). Iron limitation across chlorophyll gradients in the southern drake passage: phytoplankton responses to iron addition and photosynthetic indicators of iron stress. *Limnol. Oceanogr.* 52, 2540–2554. doi: 10.4319/lo.2007.52.6.2540

Hutchins, D. A., Witter, A. E., Butler, A., and Luther, G. W. (1999). Competition among marine phytoplankton for different chelated iron species. *Nature* 400, 858–861. doi: 10.1038/23680

Ibisanmi, E., Sander, S. G., Boyd, P. W., Bowie, A. R., and Hunter, K. A. (2011). Vertical distributions of iron-(III) complexing ligands in the Southern Ocean. *Deep Sea Res. Part II Top. Stud. Oceanogr.* 58, 2113–2125. doi: 10.1016/j.dsr2.2011.05.028

Ito, Y., and Butler, A. (2005). Structure of synechobactins, new siderophores of the marine cyanobacterium *Synechococcus* sp. PCC 7002. *Limnol. Oceanogr.* 50, 1918–1923. doi: 10.4319/lo.2005.50.6.1918

Jickells, T. D., An, Z. S., Andersen, K. K., Baker, A. R., Bergametti, G., Brooks, N., et al. (2005). Global iron connections between desert dust, ocean biogeochemistry, and climate. *Science* 308, 67–71. doi: 10.1126/science.1105959

Johnson, K. S., Elrod, V., Fitzwater, S., Plant, J., Boyle, E., Bergquist, B., et al. (2007). Developing standards for dissolved iron in seawater. *Eos Trans. AGU* 88, 131–132. doi: 10.1029/2007EO110003

Johnson, Z. I., and Lin, Y. (2009). Prochlorococcus: approved for export. *Proc. Natl. Acad. Sci. U.S.A.* 106, 10400–10401. doi: 10.1073/pnas.0905187106

Karl, D. M., and Church, M. J. (2014). Microbial oceanography and the Hawaii Ocean Time-series programme. *Nat. Rev. Microbiol.* 12, 699–713. doi: 10.1038/nrmicro3333

Karl, D. M., Church, M. J., Dore, J. E., Letelier, R. M., and Mahaffey, C. (2012). Predictable and efficient carbon sequestration in the North Pacific Ocean supported by symbiotic nitrogen fixation. *Proc. Natl. Acad. Sci. U.S.A.* 109, 1842–1849. doi: 10.1073/pnas.1120312109

Karl, D. M., and Lukas, R. (1996). The Hawaii Ocean Time-series (HOT) program: background, rationale and field implementation. *Deep Sea Res. Part II Top. Stud. Oceanogr.* 43, 129–156. doi: 10.1016/0967-0645(96)00005-7

Kem, M. P., and Butler, A. (2015). Acyl peptidic siderophores: structures, biosyntheses and post-assembly modifications. *Biometals* 28, 445–459. doi: 10.1007/s10534-015-9827-y

Kem, M. P., Naka, H., Iinishi, A., Haygood, M. G., and Butler, A. (2015). Fatty acid hydrolysis of acyl marinobactin siderophores by Marinobacter acylases. *Biochemistry* 54, 744–752. doi: 10.1021/bi5013673

King, A. L., and Barbeau, K. A. (2011). Dissolved iron and macronutrient distributions in the southern California current system. *J. Geophys. Res. Oceans* 116:18. doi: 10.1029/2010JC006324

Kondo, Y., Takeda, S., Nishioka, J., Obata, H., Furuya, K., Johnson, W. K., et al. (2008). Organic iron(III) complexing ligands during an iron enrichment experiment in the western subarctic North Pacific. *Geophys. Res. Lett.* 35:L12601. doi: 10.1029/2008GL033354

Kustka, A. B., Sa-udo-Wilhelmy, S. A., Carpenter, E. J., Capone, D., Burns, J., and Sunda, W. G. (2003). Iron requirements for dinitrogen-and ammonium-supported growth in cultures of Trichodesmium (IMS 101): comparison with nitrogen fixation rates and iron: carbon ratios of field populations. *Limnol. Oceanogr.* 48, 1869–1884. doi: 10.4319/lo.2003.48.5.1869

Lis, H., Shaked, Y., Kranzler, C., Keren, N., and Morel, F. M. (2015). Iron bioavailability to phytoplankton: an empirical approach. *ISME J.* 9, 1003–1013. doi: 10.1038/ismej.2014.199

Mahowald, N. M., Baker, A. R., Bergametti, G., Brooks, N., Duce, R. A., Jickells, T. D., et al. (2005). Atmospheric global dust cycle and iron inputs to the ocean. *Glob. Biogeochem. Cycles* 19:GB4025. doi: 10.1029/2004GB002402

Marie, D., Partensky, F., Vaulot, D., and Brussaard, C. (1999). Enumeration of phytoplankton, bacteria, and viruses in marine samples. *Curr. Protoc. Cytom.* Chapter 11:Unit 11.11. doi: 10.1002/0471142956.cy1111s10

Martinez, J. S., Carter-Franklin, J. N., Mann, E. L., Martin, J. D., Haygood, M. G., and Butler, A. (2003). Structure and membrane affinity of a suite of amphiphilic siderophores produced by a marine bacterium. *Proc. Natl. Acad. Sci. U.S.A.* 100, 3754–3759. doi: 10.1073/pnas.0637444100

Martinez, J. S., Haygood, M. G., and Butler, A. (2001). Identification of a natural desferrioxamine siderophore produced by a marine bacterium. *Limnol. Oceanogr.* 46, 420–424. doi: 10.4319/lo.2001.46.2.0420

Martinez, J. S., Zhang, G. P., Holt, P. D., Jung, H. T., Carrano, C. J., Haygood, M. G., et al. (2000). Self-assembling amphiphilic siderophores from marine bacteria. *Science* 287, 1245–1247. doi: 10.1126/science.287.5456.1245

Mawji, E., Gledhill, M., Milton, J. A., Tarran, G. A., Ussher, S., Thompson, A., et al. (2008). Hydroxamate siderophores: occurrence and importance in the Atlantic Ocean. *Environ. Sci. Technol.* 42, 8675–8680. doi: 10.1021/es801884r

Meyer, J. M., and Abdallah, M. A. (1980). The siderochromes of non-fluorescent pseudomonads: production of nocardamine by *Pseudomonas stutzeri*. *Microbiology* 118, 125–129. doi: 10.1099/00221287-118-1-125

Morel, F. M., and Price, N. M. (2003). The biogeochemical cycles of trace metals in the oceans. *Science* 300, 944–947. doi: 10.1126/science.1083545

Omanović, D., Gamier, C., and Pizeta, I. (2015). ProMCC: an all-in-one tool for trace metal complexation studies. *Mar. Chem.* 173, 25–39. doi: 10.1016/j.marchem.2014.10.011

Peterson, M. L., Wakeham, S. G., Lee, C., Askea, M. A., and Miquel, J. C. (2005). Novel techniques for collection of sinking particles in the ocean and determining their settling rates. *Limnol. Oceanogr. Methods* 3, 520–532. doi: 10.4319/lom.2005.3.520

Reid, R. T., Live, D. H., Faulkner, D. J., and Butler, A. (1993). A siderophore from a marine bacterium with an exceptional ferric ion affinity constant. *Nature* 366, 455–458. doi: 10.1038/366455a0

Roe, K. L., Barbeau, K., Mann, E. L., and Haygood, M. G. (2012). Acquisition of iron by Trichodesmium and associated bacteria in culture. *Environ. Microbiol.* 14, 1681–1695. doi: 10.1111/j.1462-2920.2011.02653.x

Rue, E. L., and Bruland, K. W. (1995). Complexation of iron(III) by natural organic-ligands in the central North Pacific as determined by a new competitive ligand equilibration adsorptive cathodic stripping voltammetric method. *Mar. Chem.* 50, 117–138. doi: 10.1016/0304-4203(95)00031-L

Schwyn, B., and Neilands, J. B. (1987). Universal chemical assay for the detection and determination of siderophores. *Anal. Biochem.* 160, 47–56. doi: 10.1016/0003-2697(87)90612-9

Shaked, Y., Kustka, A. B., and Morel, F. M. M. (2005). A general kinetic model for iron acquisition by eukaryotic phytoplankton. *Limnol. Oceanogr.* 50, 872–882. doi: 10.4319/lo.2005.50.3.0872

Shaked, Y., and Lis, H. (2012). Disassembling iron availability to phytoplankton. *Front. Microbiol.* 3:123. doi: 10.3389/fmicb.2012.00123

Shilova, I. N., Mills, M. M., Robidart, J. C., Turk-Kubo, K. A., Björkman, K. M., Kolber, Z., et al. (2017). Differential effects of nitrate, ammonium, and urea as N sources for microbial communities in the North Pacific Ocean. *Limnol. Oceanogr.* 62, 2550–2574. doi: 10.1002/lno.10590

Sunda, W. G., and Huntsman, S. A. (1997). Interrelated influence of iron, light and cell size on marine phytoplankton growth. *Nature* 390, 389–392. doi: 10.1038/37093

Tagliabue, A., Aumont, O., and Bopp, L. (2014). The impact of different external sources of iron on the global carbon cycle. *Geophys. Res. Lett.* 41, 920–926. doi: 10.1002/2013GL059059

Tagliabue, A., Aumont, O., DeAth, R., Dunne, J. P., Dutkiewicz, S., Galbraith, E., et al. (2016). How well do global ocean biogeochemistry models simulate dissolved iron distributions? *Glob. Biogeochem. Cycles* 30, 149–174. doi: 10.1002/2015GB005289

Tagliabue, A., Bowie, A. R., Boyd, P. W., Buck, K. N., Johnson, K. S., and Saito, M. A. (2017). The integral role of iron in ocean biogeochemistry. *Nature* 543, 51–59. doi: 10.1038/nature21058

Talley, L. D. (1993). Distribution and formation of North Pacific intermediate water. *J. Phys. Oceanogr.* 23, 517–537. doi: 10.1175/1520-0485(1993)023<0517:DAFONP>2.0.CO;2

Tautenhahn, R., Cho, K., Uritboonthai, W., Zhu, Z., Patti, G. J., and Siuzdak, G. (2012a). An accelerated workflow for untargeted metabolomics using the METLIN database. *Nat. Biotechnol.* 30, 826–828. doi: 10.1038/nbt.2348

Tautenhahn, R., Patti, G. J., Rinehart, D., and Siuzdak, G. (2012b). XCMS Online: a web-based platform to process untargeted metabolomic data. *Anal. Chem.* 84, 5035–5039. doi: 10.1021/ac300698c

Thompson, A. W., Huang, K., Saito, M. A., and Chisholm, S. W. (2011). Transcriptome response of high-and low-light-adapted Prochlorococcus strains to changing iron availability. *ISME J.* 5, 1580–1594. doi: 10.1038/ismej.2011.49

Tian, F., Frew, R. D., Sander, S., Hunter, K. A., and Ellwood, M. J. (2006). Organic iron. *Mar. Freshw. Res.* 57, 533–544. doi: 10.1071/MF05209

van den Berg, C. M., and Donat, J. R. (1992). Determination and data evaluation of copper complexation by organic ligands in sea water using cathodic stripping voltammetry at varying detection windows. *Anal. Chim. Acta*, 257, 281–291. doi: 10.1016/0003-2670(92)85181-5

van den Berg, C. M. G. (1995). Evidence for organic complexation of iron in seawater. *Mar. Chem.* 50, 139–157. doi: 10.1016/0304-4203(95)00032-M

Velasquez, I. B., Ibisanmi, E., Maas, E. W., Boyd, P. W., Nodder, S., and Sander, S. G. (2016). Ferrioxamine siderophores detected amongst iron binding ligands produced during the remineralization of marine particles. *Front. Mar. Sci.* 3:172. doi: 10.3389/fmars.2016.00172

Velasquez, I., Nunn, B. L., Ibisanmi, E., Goodlett, D. R., Hunter, K. A., and Sander, S. G. (2011). Detection of hydroxamate siderophores in coastal and

Sub-Antarctic waters off the South Eastern Coast of New Zealand. *Mar. Chem.* 126, 97–107. doi: 10.1016/j.marchem.2011.04.003

Vraspir, J. M., and Butler, A. (2009). Chemistry of marine ligands and siderophores. *Ann. Rev. Mar. Sci.* 1, 43–63. doi: 10.1146/annurev.marine.010908.163712

Wagener, T., Pulido-Villena, E., and Guieu, C. (2008). Dust iron dissolution in seawater: results from a one-year time-series in the Mediterranean Sea. *Geophys. Res. Lett.* 35:L16601. doi: 10.1029/2008GL034581

Witter, A. E., Hutchins, D. A., Butler, A., and Luther, G. (2000). Determination of conditional stability constants and kinetic constants for strong model Fe-binding ligands in seawater. *Mar. Chem.* 69, 1–17. doi: 10.1016/S0304-4203(99)00087-0

Conflict of Interest Statement: The authors declare that the research was conducted in the absence of any commercial or financial relationships that could be construed as a potential conflict of interest.